First-principles study on Ni_3Al (111) antiphase boundary with Ti and Hf impurities

Ruoshi Sun,[1,*] Christopher Woodward,[2] and Axel van de Walle[1]
[1]*School of Engineering, Brown University, Providence, Rhode Island 02912, USA*
[2]*Materials and Manufacturing Directorate, Air Force Research Laboratory, Wright-Patterson Air Force Base, Dayton, Ohio 45433, USA*

(Received 21 December 2016; revised manuscript received 9 April 2017; published 30 June 2017)

The effect of Ti and Hf impurities on the (111) antiphase boundary (APB) energy of Ni_3Al is investigated via *ab initio* calculations. Cluster expansion is performed to predict supercell total energies sampled in a Monte Carlo approach that accounts for nondilute point defects at finite temperature, obtaining APB energies as a function of impurity concentration and temperature. Of the two ternary elements, Hf is more effective in increasing the APB energy. While the (111) APB energy of a pure $L1_2$ material requires at least second-nearest-neighbor interactions, we observe a strong correlation between impurity-induced APB energy enhancement and formation of first-nearest-neighbor Ni-Ni bonds across the APB due to symmetry breaking. Using a linear-chain model and effective bond energies derived from effective cluster interactions, we propose a mechanism that explains why Hf is more effective than Ti.

DOI: 10.1103/PhysRevB.95.214121

I. INTRODUCTION

Ni_3Al is a technologically important material that is used for γ' precipitate strengthening in Ni-based superalloys. Further enhancement in strength can be achieved by solute additions, which has been extensively studied in experiments [1]. Computational techniques for solute-dislocation interactions have been applied successfully to predict solute strengthening [2] and solute softening [3]. In precipitates such as γ' significant strengthening occurs when an ordinary ($\frac{1}{2}[110]$) dislocation cuts the precipitate producing an antiphase boundary (APB). The resistance to shear is proportional to the APB energy, which is sensitive to composition and temperature. The Ni-Al γ'-γ phase boundary is fairly insensitive to temperature and binary composition, so the ratio of Ni to Al in Ni_3Al is fairly constant over a range of alloy compositions. However, ternary additions can strongly affect the APB energy and enhance strengthening by increasing the APB energy. Recently, the effect of off-stoichiometry [4] and that of transition-metal additions [5,6] on the APB energy of Ni_3Al have been investigated from computational approaches.

The effect of substitutional impurities on the APB energy is a subject of wide interest. Current first-principles approaches are often either mean-field-based (such as the coherent potential approximation used in Refs. [6–8]) or atomistic but not statistical (e.g., Refs. [5,9]). As far as the authors are aware, the first application of an atomistic and statistical method to APBs was used by Asta and Quong in a study on the effect of off-stoichiometry in TiAl [10]. To obtain APB energy as a function of temperature and impurity concentration, we have developed a cluster expansion (CE) method based on density functional theory (DFT) total-energy calculations and Monte Carlo (MC) sampling techniques [11]. In the current study, we apply this method to investigate the effect of Ti and Hf impurities on the $\frac{1}{2}\langle 1\bar{1}0\rangle\{111\}$ APB energy in Ni_3Al and propose an atomistic mechanism for APB energy enhancement in this system.

II. METHODS

DFT [12,13] calculations within the Perdew-Burke-Ernzerhof [14,15] generalized gradient approximation were performed using the plane-wave code Vienna Ab-initio Simulation Package (VASP) [16–19] with projector augmented wave potentials [20,21]. The semicore pseudopotential was used for Hf. To achieve accurate phase stability in the Ni-Al system, spin polarization was applied to Ni atoms [22]. Total energies were converged to within 10^{-6} and 10^{-4} eV for each self-consistent loop and ionic relaxation step, respectively, using 4000 Monkhorst-Pack k points [23] per reciprocal atom.

For the cluster expansion (CE) [24] step, 71, 142, and 107 structures were used, respectively, for the binary system Ni-Al and the ternary systems Ni-Al-Ti and Ni-Al-Hf, to express the total energy as a linear combination of effective cluster interactions (ECIs):

$$E = \sum_{\alpha} m_{\alpha} J_{\alpha} \left\langle \prod_{\alpha} \sigma_{\alpha} \right\rangle, \tag{1}$$

where the summation index α runs over clusters, m_α and J_α are the corresponding multiplicity and ECI, and the bracketed term is the cluster correlation function. A $6 \times 6 \times 5$ supercell of the 12-atom (111)-oriented unit cell was used for the MC simulation, performed at temperatures between 800 K and 1600 K and impurity concentrations between 0.5% and 10%. We used the Alloy Theoretic Automated Toolkit (ATAT) software package [11,25,26] for CE and MC. Further computational details can be found in Ref. [11].

An APB has the desirable property of not breaking the symmetry of the system's underlying lattice; in other words, the set of all atomic sites (regardless of their occupation) forms the parent lattice even in the presence of the APB. As a result, a standard, translation-independent cluster expansion can be used to represent the energetics of the system. We define the

*ruoshi@alum.mit.edu

APB energy as

$$\gamma = \frac{E - 2E_0}{2A} = \frac{N(e - e_0)}{A}, \tag{2}$$

where e_0 and e are in units of energy per atom, N is the number of atoms, and A is the cross-sectional area of the supercell. The effectiveness of solute additions is assessed by the enhancement in the APB energy:

$$\Delta\gamma(x) = \gamma(x) - \gamma(0), \tag{3}$$

where x is the impurity concentration. Contributions from vibrational entropy have been found to be small in this system [4,27] and thus are not considered.

III. RESULTS

A. Enhancement of APB energy by impurities

For the pure Ni_3Al system, its equilibrium lattice constant from DFT and APB energy from CE are in good agreement with the literature, as reported in our earlier work [11]. The ECIs for the binary Ni-Al and ternary Ni-Al-Ti and Ni-Al-Hf systems are plotted as a function of the cluster diameter in Fig. 1. The CE for the Ni-Al-Hf system has a cross-validation (CV) score of 33.0 meV/atom, slightly higher than that for the Ni-Al-Ti system (30.4 meV/atom). The APB energy of pure Ni_3Al obtained from CE of the binary Ni-Al system is 318 mJ/m^2. In addition to the agreement with the unrelaxed first-principles value of 300 mJ/m^2 reported in Ref. [4] versus 344 mJ/m^2 from our calculations, we validate further by relaxing all internal degrees of freedom at constant volume and cell shape. We obtain an APB energy of 217 mJ/m^2,

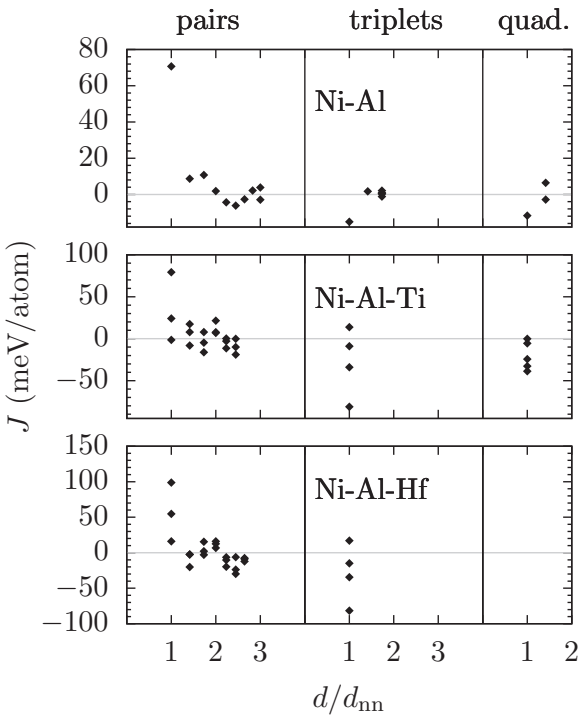

FIG. 1. Effective cluster interaction J as a function of cluster diameter d normalized by nearest-neighbor distance d_{nn} for (top) Ni-Al, (middle) Ni-Al-Ti, and (bottom) Ni-Al-Hf systems.

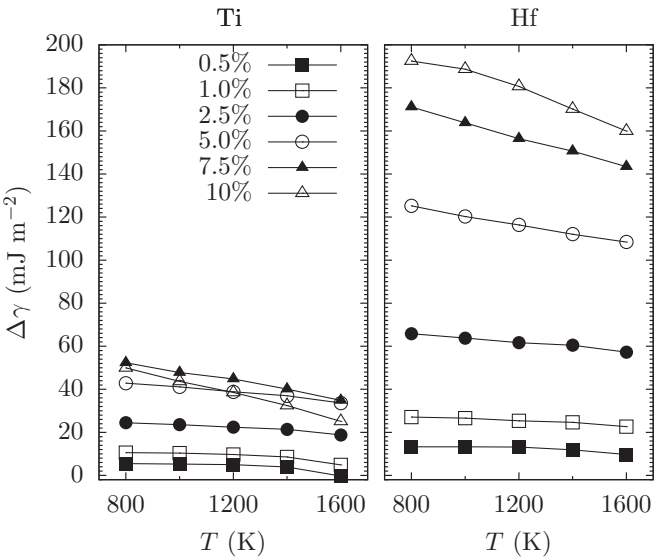

FIG. 2. Effect of 0.5%–10% (left) Ti and (right) Hf on the mean APB energy of Ni_3Al as a function of temperature.

corresponding to an error of 16.4 meV/atom, which is consistent with the CV score.

The enhancement of APB energy by impurity X [Eq. (3)] is obtained from CE of the ternary Ni-Al-X system. The reference APB energy, $\gamma(0)$, is 248 and 259 mJ/m^2 for Ni-Al-Ti and Ni-Al-Hf, respectively, which has a much smaller discrepancy with respect to the DFT APB energy of 217 mJ/m^2 than the binary CE reference APB energy as reported in the previous paragraph. To formally assess the error cancellation, we compare the difference in the APB energy of pure Ni_3Al obtained from CE and DFT versus that of Ni_3Al:Ti, i.e., $|(\gamma^{CE}_{pure} - \gamma^{DFT}_{pure}) - (\gamma^{CE}_{imp} - \gamma^{DFT}_{imp})|$. Values for the first bracketed term are already available: $\gamma^{CE}_{pure} = 248$ mJ/m^2 and $\gamma^{DFT}_{pure} = 217$ mJ/m^2. For the second bracketed term, we use a $2 \times 2 \times 2$ (111)-oriented cell with composition $Ni_{72}Al_{23}Ti$, where the impurity is placed near the interface. The APB energies are $\gamma^{CE}_{imp} = 287$ mJ/m^2 and $\gamma^{DFT}_{imp} = 253$ mJ/m^2. The absolute difference between the two bracketed terms is 3 mJ/m^2. Although this value may not reflect the accuracy of CE for every atomic configuration, it is indicative of the accuracy of our predicted effect of impurities and the presence of significant error cancellation. Results presented henceforth are based on ternary CEs.

Using the ternary ECIs, MC sampling of the mean APB energy change is plotted in Fig. 2 as a function of temperature for each impurity concentration. For Ti, maximum enhancement in the APB energy is achieved at 7.5 at. % within the considered temperature range (800 K to 1600 K), where $\Delta\gamma$ is above 50 mJ m^{-2}. Adding 10 at. % Ti is less beneficial such that $\Delta\gamma$ is even smaller compared to adding 5 at. % above 1200 K. On the other hand, Hf is predicted to enhance the APB energy drastically. A concentration of 2.5 at. % already outperforms the maximum effect of Ti, and the rate of increase in APB energy gradually reduces as Hf concentration increases to 10 at. %, where the enhancement is above 190 mJ m^{-2}. This result suggests that Hf is a more effective candidate than Ti, which agrees with experimental findings [28].

In the following subsections, we address the mechanism by which the addition of Hf is so effective in increasing the APB energy.

B. Correlation to impurity coverage near APB

While the simulations presented in the previous section include the effects of all possible configurational mechanisms on the APB energy, it is instructive to isolate the dominant mechanism. Atomistic simulations enable a formal and detailed investigation of this question. Our general approach is to identify structural features that best correlate with APB energy enhancement. Specifically, we use the Pearson correlation, defined as

$$\rho_{\Delta\gamma,X} = \frac{\mathrm{cov}(\Delta\gamma, X)}{\sigma_{\Delta\gamma}\sigma_X}, \tag{4}$$

where σ is the standard deviation, to further investigate the structural effect on APB energy by analyzing the correlation between $\Delta\gamma$ and some other variable of interest, X. Here, values of ρ range from -1 to 1, where $\rho = 0$, $\rho > 0$, and $\rho < 0$ indicate no linear correlation, positive linear correlation, and negative linear correlation, respectively. (Nonlinear effects were verified to be negligible by fitting to a fifth-order polynomial.) The Pearson correlation is widely used in the literature. For instance, in a high-throughput computational study by Pilania *et al.* [29], it is used to distinguish strong versus weak correlation between various physical properties.

In this subsection, we consider the coverage of impurity atoms in the nearest and second-nearest planes to the APB, where $X = \theta_1$ and θ_2, respectively. Since the Pearson coefficient is invariant under scaling and constant shift, the actual APB energy γ and the number of impurity atoms near the APB can be used directly in Eq. (4). The $\Delta\gamma$ subscript is dropped from ρ hereafter.

The correlations are computed from all the sampled structures in MC and plotted as a function of temperature in Fig. 3 at the extreme impurity concentrations (0.5% and 10%).

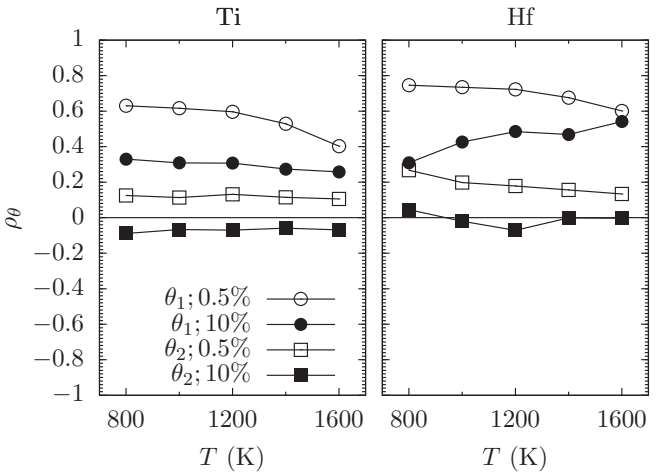

FIG. 3. Correlation between APB energy and the coverage of (left) Ti and (right) Hf impurity atoms in the nearest plane (θ_1) and second-nearest plane (θ_2) as a function of temperature. For clarity, only the correlations at 0.5% and 10% impurity concentrations are shown. Correlations at intermediate concentrations are listed in Table I.

TABLE I. Correlation between APB energy and the coverage of Ti and Hf impurity atoms in the nearest plane (θ_1) and the second-nearest plane (θ_2).

		Ti		Hf	
x (%)	T (K)	θ_1	θ_2	θ_1	θ_2
0.5	800	0.63	0.13	0.75	0.27
	1000	0.62	0.11	0.73	0.20
	1200	0.60	0.13	0.72	0.18
	1400	0.53	0.11	0.68	0.16
	1600	0.40	0.11	0.60	0.13
1.0	800	0.63	0.07	0.77	0.21
	1000	0.62	0.08	0.77	0.17
	1200	0.63	0.08	0.74	0.19
	1400	0.57	0.07	0.69	0.15
	1600	0.48	0.08	0.66	0.13
2.5	800	0.60	0.03	0.78	0.20
	1000	0.61	0.05	0.77	0.16
	1200	0.58	0.04	0.74	0.17
	1400	0.57	0.05	0.74	0.14
	1600	0.54	0.06	0.73	0.14
5.0	800	0.54	−0.03	0.67	−0.01
	1000	0.53	−0.07	0.71	0.06
	1200	0.53	−0.06	0.69	0.04
	1400	0.51	0.02	0.72	0.05
	1600	0.47	0.01	0.71	0.01
7.5	800	0.47	−0.10	0.53	−0.06
	1000	0.42	−0.09	0.57	−0.03
	1200	0.43	−0.05	0.60	−0.01
	1400	0.41	−0.05	0.61	−0.05
	1600	0.39	−0.07	0.61	0.03
10	800	0.33	−0.09	0.31	0.05
	1000	0.31	−0.07	0.43	−0.02
	1200	0.31	−0.07	0.49	−0.07
	1400	0.27	−0.06	0.47	0.00
	1600	0.26	−0.07	0.54	0.00

Results at intermediate concentrations are shown in Table I. For both Ti and Hf, coverage of the nearest layer to the APB has a stronger correlation than that of the second-nearest layer. The correlation value ρ_{θ_1} is the highest at 0.5% Ti and 2.5% Hf at 800 K, being 0.63 and 0.78, respectively. In general, ρ_{θ_1} decreases with increasing impurity concentration and reaches a minimum at 10%. This result suggests that impurity coverage of the nearest layer is only somewhat responsible for the enhancement in the APB energy, especially since ρ_{θ_1} can drop to values around 0.3 at 10% impurity concentration, and that there may be other possible mechanisms for APB energy enhancement. Correlation between the enhancement in APB energy and impurity coverage of the second-nearest layer is weak, since $|\rho_{\theta_2}|$ is within 0.3.

We remark that ρ_{θ_1} is not predictive since, for instance, its peak value is obtained for 2.5% Hf at 800 K, but the maximum $\Delta\gamma$ occurs at 10% Hf (Fig. 2).

C. Correlation to bonding across APB

For the $L1_2$ structure, the number of each type of nearest-neighbor bonds is invariant upon formation of the

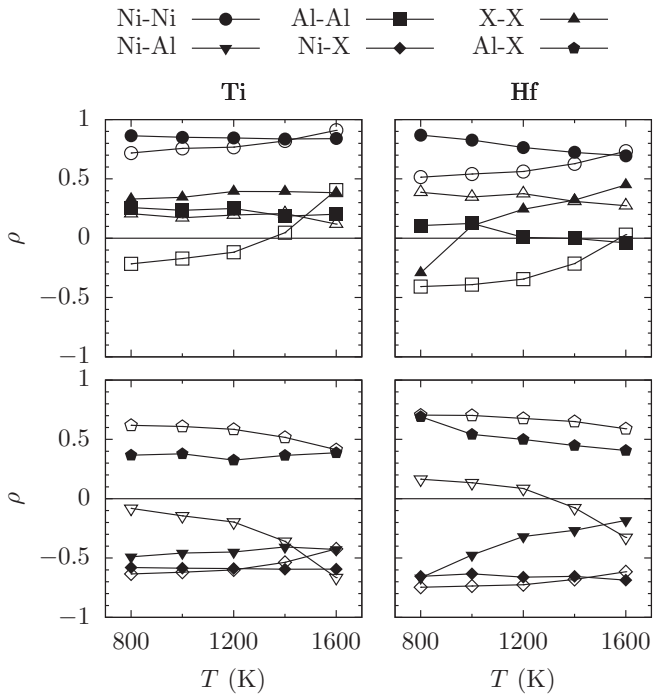

FIG. 4. Correlation between APB energy and net number of first-nearest-neighbor bonds formed across the APB as a function of temperature for (left) Ti and (right) Hf at 0.5% (open symbols) and 10% (solid symbols) concentrations. Self-pairs and cross-pairs are shown in the top and bottom panels, respectively. Correlations at intermediate Ti and Hf concentrations are listed in Tables II and III, respectively.

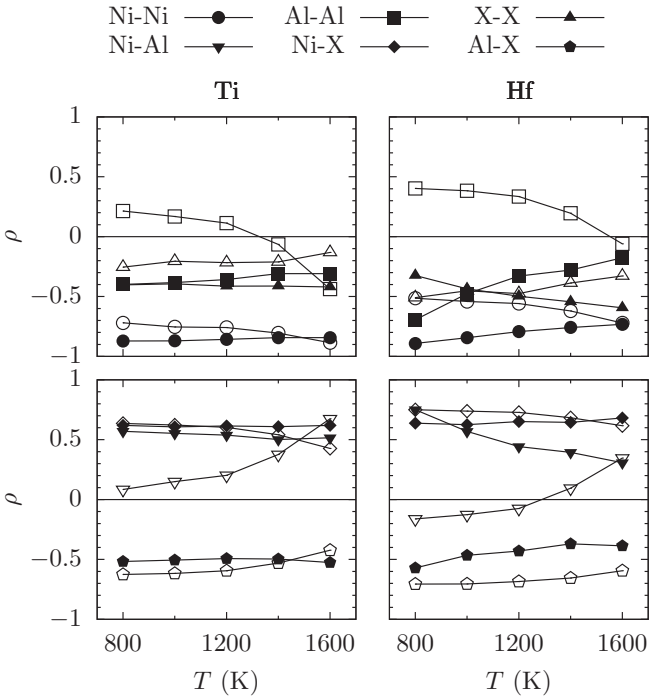

FIG. 5. Correlation between APB energy and net number of second-nearest-neighbor bonds formed across the APB as a function of temperature for (left) Ti and (right) Hf at 0.5% (open symbols) and 10% (solid symbols) concentrations. Self-pairs and cross-pairs are shown in the top and bottom panels, respectively. Correlations at intermediate Ti and Hf concentrations are listed in Tables II and III, respectively.

$\frac{1}{2}\langle 1\bar{1}0\rangle\{111\}$ APB. Thus, at least second-nearest neighbors must be used in the cluster expansion of the APB structure of pure Ni_3Al. Here, we examine the net number of first- and second-nearest-neighbor bonds formed across the APB. A positive (negative) value indicates net bond forming (breaking) between two species X and Y upon formation of the APB. Only the first- and second-nearest planes adjacent to the APB are considered. In-plane bonds are not affected and can thus be ignored. The correlation between APB energy and first- and second-nearest-neighbor bonds across the APB is shown in Figs. 4 and 5, respectively, as a function of temperature at the extreme impurity concentrations (0.5% and 10%). Results at intermediate Ti and Hf concentrations are shown in Tables II and III, respectively.

1. First-nearest-neighbor bonds

While first-nearest-neighbor bonds do not contribute to the (111) APB energy for pure Ni_3Al, the local symmetry in the vicinity of the APB is broken when impurities are introduced. Indeed, from Fig. 4, the magnitude of the correlation is not only different from 0 but also very high in several cases. We examine all possible pairs below in the order of self-pairs (Ni-Ni, Al-Al, X-X) followed by cross-pairs (Ni-Al, Al-X, Ni-X).

(a) Ni-Ni. For both Ni_3Al:Ti and Ni_3Al:Hf systems, strong correlation is observed between APB energy enhancement and formation of Ni-Ni first-nearest-neighbor bonds. In the case of Ti, the correlation is weakly dependent on impurity concentration and temperature, ranging from 0.72 (0.5% at 800 K) to 0.91 (0.5% at 1600 K). In the case of Hf, the correlation becomes stronger with increasing impurity concentration, reaching a maximum of 0.87 (10% at 800 K).

(b) Al-Al. The correlation is weak in both systems, where the magnitude is within about 0.4.

(c) X-X. In the case of Ti, the correlation is stronger at higher impurity concentrations, being around 0.4 for 5%–10%. In the case of Hf, it is the highest at 2.5%–5%, being around 0.5.

(d) Ni-Al. For Ti, the correlation becomes stronger (more negative) with increasing temperature at low impurity concentration, reaching a moderate value of −0.665 (0.5% at 1600 K). For Hf, the correlation generally becomes stronger with decreasing temperature, reaching a moderate value of −0.667 (10% at 800 K).

(e) Ni-X. Moderately strong correlation is observed for the breaking of Ni-X bonds in both systems. The value is relatively insensitive to temperature and concentration, being around −0.6 for Ti and −0.7 for Hf.

(f) Al-X. In both systems, the correlation decreases with increasing concentration. The highest value is 0.62 for Ti (0.5% at 800 K) and 0.71 for Hf (1.0% at 800 K).

For all the first-nearest-neighbor bonds, the correlation is the highest for Ni-Ni bond forming, followed by Ni-X and Al-X bond breaking.

2. Second-nearest-neighbor bonds

Compared to the correlation of first-nearest-neighbor bonds, that of second-nearest-neighbor bonds, in general, is opposite in sign but similar in magnitude.

TABLE II. Correlation between APB energy and net number of first- and second-nearest-neighbor bonds formed across the APB for Ni_3Al:Ti.

		First-nearest-neighbor bonds						Second-nearest-neighbor bonds					
x (%)	T (K)	Ni-Ni	Al-Al	Ti-Ti	Ni-Al	Ni-Ti	Al-Ti	Ni-Ni	Al-Al	Ti-Ti	Ni-Al	Ni-Ti	Al-Ti
0.5	800	0.72	−0.22	0.21	−0.08	−0.63	0.62	−0.72	0.21	−0.25	0.08	0.64	−0.63
	1000	0.76	−0.17	0.17	−0.14	−0.62	0.61	−0.75	0.17	−0.21	0.15	0.62	−0.62
	1200	0.77	−0.12	0.20	−0.20	−0.60	0.58	−0.76	0.11	−0.22	0.20	0.60	−0.59
	1400	0.82	0.05	0.21	−0.36	−0.54	0.52	−0.81	−0.07	−0.21	0.38	0.54	−0.53
	1600	0.91	0.41	0.12	−0.66	−0.42	0.41	−0.89	−0.44	−0.13	0.67	0.43	−0.42
1.0	800	0.77	−0.16	0.28	−0.15	−0.63	0.60	−0.76	0.17	−0.29	0.15	0.64	−0.63
	1000	0.77	−0.15	0.27	−0.15	−0.62	0.60	−0.77	0.15	−0.30	0.16	0.63	−0.62
	1200	0.78	−0.15	0.25	−0.18	−0.64	0.61	−0.77	0.14	−0.30	0.19	0.64	−0.62
	1400	0.83	−0.00	0.23	−0.33	−0.58	0.56	−0.81	−0.02	−0.27	0.35	0.58	−0.57
	1600	0.87	0.21	0.21	−0.51	−0.51	0.49	−0.85	−0.25	−0.24	0.53	0.51	−0.50
2.5	800	0.81	−0.07	0.38	−0.22	−0.61	0.54	−0.80	0.08	−0.41	0.23	0.64	−0.60
	1000	0.80	−0.08	0.38	−0.21	−0.62	0.54	−0.80	0.08	−0.40	0.23	0.64	−0.61
	1200	0.82	−0.03	0.36	−0.26	−0.60	0.52	−0.81	0.02	−0.39	0.29	0.62	−0.58
	1400	0.83	−0.01	0.35	−0.29	−0.60	0.53	−0.82	−0.01	−0.38	0.33	0.62	−0.59
	1600	0.85	0.08	0.36	−0.37	−0.56	0.50	−0.84	−0.11	−0.38	0.42	0.59	−0.55
5.0	800	0.86	0.12	0.41	−0.36	−0.58	0.41	−0.86	−0.13	−0.46	0.40	0.63	−0.55
	1000	0.84	0.07	0.41	−0.32	−0.58	0.43	−0.84	−0.09	−0.44	0.36	0.62	−0.56
	1200	0.84	0.07	0.41	−0.31	−0.58	0.43	−0.84	−0.09	−0.44	0.36	0.61	−0.54
	1400	0.85	0.09	0.38	−0.35	−0.57	0.43	−0.85	−0.12	−0.41	0.40	0.60	−0.55
	1600	0.86	0.13	0.38	−0.39	−0.56	0.44	−0.85	−0.18	−0.39	0.45	0.59	−0.55
7.5	800	0.87	0.20	0.38	−0.43	−0.58	0.38	−0.88	−0.26	−0.44	0.49	0.63	−0.55
	1000	0.86	0.22	0.38	−0.43	−0.55	0.35	−0.87	−0.29	−0.41	0.50	0.59	−0.49
	1200	0.86	0.16	0.40	−0.38	−0.57	0.39	−0.86	−0.24	−0.43	0.46	0.60	−0.50
	1400	0.85	0.15	0.41	−0.38	−0.58	0.39	−0.86	−0.23	−0.41	0.46	0.61	−0.53
	1600	0.86	0.18	0.40	−0.42	−0.58	0.40	−0.86	−0.25	−0.41	0.49	0.62	−0.55
10	800	0.86	0.26	0.33	−0.49	−0.58	0.37	−0.87	−0.40	−0.40	0.57	0.62	−0.52
	1000	0.85	0.24	0.34	−0.46	−0.59	0.38	−0.87	−0.38	−0.39	0.55	0.61	−0.51
	1200	0.85	0.25	0.39	−0.45	−0.59	0.33	−0.86	−0.36	−0.41	0.54	0.61	−0.49
	1400	0.84	0.19	0.39	−0.41	−0.59	0.36	−0.84	−0.31	−0.41	0.50	0.61	−0.50
	1600	0.84	0.20	0.38	−0.43	−0.59	0.39	−0.84	−0.31	−0.42	0.52	0.62	−0.53

(a) Ni-Ni. Strong correlation is observed in both systems. For Ti, the correlation is relatively insensitive to concentration and temperature, ranging from −0.72 (0.5% at 800 K) to −0.89 (0.5% at 1600 K). It is more sensitive in the Hf system; with increasing temperature, it becomes weaker (less negative) at high concentration but stronger (more negative) at low concentration, spanning a wider ranger from −0.49 (1.0% at 800 K) to −0.89 (10% at 800 K).

(b) Al-Al. For Ti, the correlation is weak since its magnitude is within about 0.4. For Hf, it is weak at most concentrations and temperatures, but reaches a moderate value of −0.69 at 10% at 800 K.

(c) X-X. The correlation is again weak for Ti with a magnitude of about 0.4. For Hf, it is moderate at 2.5%–5%, approaching −0.7.

(d) Ni-Al. For Ti, the correlation is moderate (around 0.5) at 10%, attaining the maximum value of 0.67 at 0.5% at 1600 K. For Hf, the correlation is the strongest (0.75) at high concentration and low temperature.

(e) Ni-X. For both systems, the correlation is relatively insensitive to temperature and concentration, being around 0.6 for Ti and 0.7 for Hf.

(f) Al-X. Moderate correlation is observed, ranging from about −0.5 to −0.6 for Ti and about −0.4 to −0.7 for Hf.

Among all the second-nearest-neighbor bonds, the strongest correlation is found for Ni-Ni bond breaking. All the cross-pairs (Ni-Al forming, Ni-X forming, Al-X breaking) exhibit moderate correlation.

D. Mechanism of APB energy enhancement

1. *Effective bond energy*

To assess the atomistic mechanism of APB enhancement, here we define an effective bond energy β based on the ECIs of nearest-neighbor pair clusters. We show how it can be applied in the next subsection.

From Eq. (1), the energy of a cluster α is

$$E_\alpha = J_\alpha \left\langle \prod_\alpha \sigma_\alpha \right\rangle. \tag{5}$$

When a cluster α contains only a pair of atoms, m and n, each of which can take values of 1 (Ni), 2 (Al), or 3 (X), we use β_{mn} to denote the effective bond energy.

TABLE III. Correlation between APB energy and net number of first- and second-nearest-neighbor bonds formed across the APB for Ni_3Al:Hf.

		First-nearest-neighbor bonds						Second-nearest-neighbor bonds					
x (%)	T (K)	Ni-Ni	Al-Al	Hf-Hf	Ni-Al	Ni-Hf	Al-Hf	Ni-Ni	Al-Al	Hf-Hf	Ni-Al	Ni-Hf	Al-Hf
0.5	800	0.51	−0.41	0.39	0.16	−0.75	0.70	−0.51	0.40	−0.51	−0.16	0.75	−0.71
	1000	0.54	−0.39	0.35	0.13	−0.74	0.70	−0.54	0.38	−0.45	−0.13	0.74	−0.70
	1200	0.56	−0.34	0.38	0.09	−0.73	0.68	−0.56	0.33	−0.48	−0.07	0.73	−0.68
	1400	0.63	−0.21	0.31	−0.08	−0.68	0.65	−0.62	0.20	−0.39	0.10	0.68	−0.66
	1600	0.73	0.03	0.27	−0.33	−0.62	0.59	−0.72	−0.06	−0.33	0.35	0.62	−0.59
1.0	800	0.49	−0.43	0.49	0.20	−0.77	0.71	−0.49	0.42	−0.60	−0.19	0.78	−0.72
	1000	0.56	−0.40	0.46	0.15	−0.77	0.70	−0.56	0.39	−0.57	−0.13	0.78	−0.72
	1200	0.56	−0.36	0.44	0.11	−0.75	0.68	−0.56	0.35	−0.55	−0.09	0.75	−0.69
	1400	0.59	−0.26	0.39	0.00	−0.70	0.64	−0.59	0.24	−0.49	0.02	0.71	−0.66
	1600	0.67	−0.14	0.36	−0.15	−0.68	0.63	−0.66	0.10	−0.46	0.18	0.68	−0.64
2.5	800	0.52	−0.41	0.51	0.19	−0.79	0.68	−0.50	0.37	−0.68	−0.16	0.80	−0.70
	1000	0.57	−0.37	0.53	0.14	−0.77	0.65	−0.56	0.35	−0.67	−0.11	0.79	−0.69
	1200	0.58	−0.31	0.51	0.08	−0.75	0.62	−0.58	0.29	−0.64	−0.05	0.76	−0.66
	1400	0.60	−0.29	0.53	0.05	−0.74	0.63	−0.60	0.27	−0.63	−0.01	0.77	−0.67
	1600	0.62	−0.23	0.53	−0.02	−0.74	0.62	−0.61	0.20	−0.63	0.05	0.76	−0.65
5.0	800	0.65	−0.14	0.43	−0.09	−0.70	0.49	−0.63	0.02	−0.64	0.17	0.74	−0.52
	1000	0.65	−0.20	0.50	−0.03	−0.74	0.52	−0.64	0.12	−0.68	0.09	0.77	−0.54
	1200	0.64	−0.19	0.49	−0.03	−0.72	0.52	−0.64	0.12	−0.66	0.09	0.75	−0.55
	1400	0.65	−0.21	0.55	−0.01	−0.75	0.52	−0.66	0.14	−0.68	0.07	0.77	−0.58
	1600	0.67	−0.19	0.54	−0.05	−0.74	0.54	−0.68	0.11	−0.67	0.12	0.77	−0.59
7.5	800	0.76	0.04	0.24	−0.32	−0.64	0.44	−0.76	−0.28	−0.55	0.42	0.67	−0.41
	1000	0.74	0.01	0.31	−0.27	−0.66	0.45	−0.74	−0.20	−0.57	0.34	0.70	−0.44
	1200	0.72	−0.06	0.39	−0.18	−0.69	0.46	−0.74	−0.11	−0.59	0.28	0.71	−0.48
	1400	0.72	−0.05	0.46	−0.18	−0.70	0.44	−0.74	−0.10	−0.63	0.27	0.72	−0.46
	1600	0.71	−0.09	0.49	−0.13	−0.71	0.45	−0.72	−0.05	−0.63	0.23	0.72	−0.48
10	800	0.87	0.11	−0.29	−0.67	−0.65	0.69	−0.89	−0.69	−0.32	0.75	0.64	−0.57
	1000	0.83	0.12	0.11	−0.47	−0.63	0.54	−0.84	−0.48	−0.44	0.57	0.63	−0.47
	1200	0.76	0.01	0.24	−0.32	−0.66	0.50	−0.79	−0.33	−0.50	0.44	0.65	−0.43
	1400	0.72	−0.00	0.32	−0.27	−0.65	0.45	−0.76	−0.28	−0.54	0.39	0.64	−0.37
	1600	0.70	−0.04	0.45	−0.18	−0.69	0.41	−0.73	−0.18	−0.59	0.31	0.68	−0.39

The calculated β values for point terms and first-nearest-neighbor bonds in both Ti and Hf systems are given in Table IV. We emphasize that the β values by themselves are not meaningful as they contain point-term ECIs and that only differences, obtained by computing the reaction energy at a constant number of each atomic species, provide desirable information. In the next subsection, we use these effective bond energies to provide a quantitative analysis of the mechanism for APB energy enhancement and the differences between Ti and Hf impurities.

2. *Mechanism*

In Sec. III C 1, we have shown that the enhancement in the APB energy is strongly correlated with the formation of Ni-Ni first-nearest-neighbor bonds across the APB. This result may seem unintuitive at first, since the number of each type of first-nearest-neighbor bonds is conserved during the formation of a $\frac{1}{2}\langle 1\bar{1}0\rangle\{111\}$ APB in a pure $L1_2$ structure. Moreover, consider the simple linear-chain reaction model with only nearest-neighbor interactions:

$$\text{Ni-Al-Ni} \rightarrow \text{Ni-Ni-Al}, \tag{6}$$

where a schematic is drawn in Fig. 6. In this process, the initial state has an energy of $2\beta_{12} - \beta_2$ and the final state has an energy of $\beta_{11} + \beta_{12} - \beta_1$. The reaction energy is thus $\beta_{11} - \beta_{12} - \beta_1 + \beta_2$. Subsituting the values from Table IV, we obtain -0.023 eV, meaning that the formation of Ni-Ni first-nearest-neighbor bonds is actually energetically favorable. This result is in agreement with the finding that the Ni-Ni_3Al interfacial

TABLE IV. Calculated β values (in eV) for point terms and first-nearest-neighbor bonds in the Ni_3Al:X system.

X	β_1 (Ni)	β_2 (Al)	β_3 (X)	β_{11} (Ni-Ni)	β_{22} (Al-Al)	β_{33} (X-X)	β_{23} (Al-X)	β_{13} (Ni-X)	β_{12} (Ni-Al)
Ti	−0.481	−0.482	−0.062	−0.962	−0.926	−0.044	−0.604	−0.563	−0.941
Hf	−0.602	−0.425	0.459	−1.143	−0.843	1.063	−0.012	−0.244	−0.988

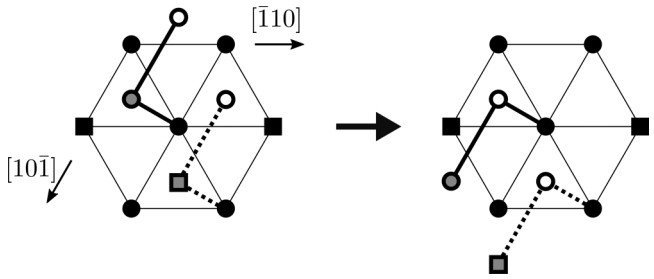

FIG. 6. Schematic of the reaction in Eqs. (6) and (7) projected onto the (111) plane. Solid and open symbols represent atoms in the lower and upper (111) planes, respectively. Circles (squares) indicate Ni (Al) sites. A shaded circle (square) in the upper plane represents an impurity X on the Ni (Al) site, whose chain is drawn in thick solid (dotted) lines. When an APB is created along the [10$\bar{1}$] direction, a Ni-Ni first-nearest-neighbor bond is formed in both X_{Ni} and X_{Al} cases. Equation (6) corresponds to the change in the dotted chain without impurity substitution on the Al site.

boundary, across which Ni-Ni bonds are formed, can have a lower energy than the APB energy of Ni_3Al [30].

However, if impurities are present at the vicinity of the APB, one must consider another possibility (Fig. 6):

$$\text{Ni-}X\text{-Ni} \rightarrow \text{Ni-Ni-}X, \tag{7}$$

with reaction energy $\beta_{11} - \beta_{13} - \beta_1 + \beta_3$, which, from Table IV, is equal to 0.019 eV for Ti and 0.162 eV for Hf. This result may explain why the addition of Hf is much more effective than that of Ti at all concentrations (Fig. 2).

On the other hand, the formation of impurity X-X bonds across the APB may seem to be a more intuitive mechanism in the sense that the overlap of impurity-induced elastic fields should be energetically unfavorable. This is verified by considering the linear-chain model:

$$X\text{-}H\text{-}X \rightarrow X\text{-}X\text{-}H, \tag{8}$$

where H represents a host atom (Ni, Al). The reaction energy is $\beta_{33} - \beta_{13} - \beta_3 + \beta_1$ and is summarized in Table V, which shows that Hf atoms tend to avoid each other more than Ti atoms do. While the formation of the Hf-Hf bond is indeed more energetically unfavorable than that of Ti-Ti, its correlation to APB energy enhancement is only moderate when compared to that of Ni-Ni (Fig. 4).

E. Site preference

As another application of effective bond energies, the site preference of an impurity X in the $L1_2$ host A_3B can be obtained as follows. Consider the substitutional reaction

$$X_B + A_A \rightarrow X_A + A_B, \tag{9}$$

where subscripts A and B represent Ni and Al sites, respectively. Note that in the $L1_2$ structure the A site has 4 B and 8 A nearest neighbors and that the B site has 12 A nearest neighbors. The reaction energy is expressed conveniently as

$$\begin{aligned}\Delta E_{\text{rxn}} &= 4\beta_{23} + 8\beta_{13} + 12\beta_{11} - (4\beta_{12} + 8\beta_{11} + 12\beta_{13}) \\ &= 4(\beta_{11} + \beta_{23} - \beta_{12} - \beta_{13}).\end{aligned} \tag{10}$$

(The ECI point terms cancel out exactly in this procedure.) Equation (9) can be rewritten more abstractly as

$$(32)(11) \rightarrow (31)(12). \tag{11}$$

Compared with Eq. (10), the reaction energy is proportional to the difference between the sum of inner and outer pairs (right-hand side: 11, 23; left-hand side: 12, 13). Similarly, the other substitutional reaction,

$$\begin{aligned}X_A + B_B &\rightarrow X_B + B_A, \\ (31)(22) &\rightarrow (32)(21),\end{aligned} \tag{12}$$

has a reaction energy of

$$\Delta E_{\text{rxn}} = 4(\beta_{22} + \beta_{13} - \beta_{12} - \beta_{23}). \tag{13}$$

The correspondence between the index pairs and substitutional reaction energy is a special property of the $L1_2$ structure due to the ratio of nearest-neighbor species.

Using the effective bond energies in Table IV, the site preference of Ti and Hf impurities in Ni_3Al are obtained from the above energetics analysis. Reaction energies for site substitution are given in Table VI. By comparing the sign of reaction energies, the Ni (Al) site is preferred for Ti (Hf) substitution.

TABLE V. Reaction energies (in meV) for formation of X-X first-nearest-neighbor bonds in Eq. (8).

	X	
Host atom	Ti	Hf
Ni	100	246
Al	140	191

TABLE VI. Reaction energies (in meV) for site substitution by impurity X.

X	$X_{Al} + Ni_{Ni} \rightarrow X_{Ni} + Ni_{Al}$	$X_{Ni} + Al_{Al} \rightarrow X_{Al} + Al_{Ni}$
Ti	− 250	226
Hf	309	− 351

IV. DISCUSSION

This study involves two main parts: (1) modeling of impurities and (2) investigating the mechanism of APB energy enhancement. In this section, we discuss the highlights and limitations of our approach from these two perspectives.

Regarding the modeling of impurities for APB energetics, typical methods use total-energy calculations of a few selected structures (e.g., Ref. [9]) or the coherent potential approximation (e.g., Ref. [6]). Due to the vast number of possible structures, the former method cannot provide accurate statistics with current computing capabilities. The latter method, being a mean-field-type technique, avoids the statistical problem, but trades off with atomistic details. In contrast, the CE-MC

approach used in this study is both statistical and atomistic by definition, but the drawback is that long-range elastic effects cannot be captured. Nonetheless, the APB energy predicted from CE is an important quantity that can be validated by comparing to total-energy calculations [11].

As for the mechanism of APB energy enhancement, the coverage of impurities near the APB is naturally assumed to be responsible for such an effect. Indeed, if the impurity were located deep within the bulk, the APB energy would not be affected. Given that first-nearest-neighbor bonds are not involved in (111) APBs of pure $L1_2$, impurity coverage at the APB is necessary for APB energy enhancement, but the exact mechanism requires deeper investigation. Using a statistical approach, correlations with various quantities can be examined in detail. In particular, Ni-Ni first-nearest-neighbor bond formation across the APB has a higher correlation to APB energy enhancement than impurity coverage does, revealing that local structure (i.e., arrangement of atoms) can play a more important role than local chemistry alone (i.e., atomic species). The mechanism proposed in Eq. (7) is a result of comparing all first-nearest-neighbor bonds. While certain second-nearest-neighbor bonds also have high correlation to APB energy enhancement, their ECIs are much smaller in magnitude (Fig. 1) than first-nearest-neighbor ECIs. Triplet ECIs in both ternary systems are comparable in magnitude to first-nearest-neighbor pair ECIs, suggesting that local structures of higher complexity may influence the APB energy as well. To tackle the general problem of identifying complex structures at the vicinity of the APB, a machine-learning approach is suitable for further study. Although simplistic, the linear-chain model of reaction energies presented in Sec. III D 2 is still useful for a first-step analysis of other materials.

The formal procedure of using effective bond energy to predict site preference has been outlined in Secs. III D 1 and III E. We do not attempt to resolve the conflicting results of site preference in the literature (e.g., reported in Ref. [1]) as some of these differences may be the result of considering different compositions of the host structure.

Finally, we note that theoretical studies of mechanical behaviors such as yield-stress anomaly and ductility often involve ratios of APB energies corresponding to various slip systems, which are used in stability maps derived from mesoscale dislocation theory [31,32]. The method presented in this paper can be extended to investigate the temperature dependence or the concentration dependence of these phenomena from first principles.

V. CONCLUSIONS

We have presented a first-principles Monte Carlo approach to investigate the effects of Ti and Hf impurities on APB energies of Ni_3Al. The (111) APB energy is increased by both solute additions, where Hf addition leads to stronger enhancement. APB energy enhancement is positively correlated to impurity coverage of the APB, and a strong correlation to formation of first-nearest-neighbor Ni-Ni bonds is observed. Based on a linear-chain model, the enhancement mechanism is proposed as an impurity-activated process, Ni-X-Ni $\rightarrow$ Ni-Ni-X, where the reaction energy is 19 meV for Ti and 162 meV for Hf.

ACKNOWLEDGMENTS

This work was supported by the Air Force Research Laboratory via UES, Inc. under Contract No. S-992-009-004. Computational resources were provided by the Center for Computation and Visualization at Brown University and the Extreme Science and Engineering Discovery Environment (XSEDE) from the National Science Foundation under Grant No. ACI-1053575.

[1] N. S. Stoloff, Int. Mater. Rev. **34**, 153 (1989).
[2] G. P. M. Leyson, W. A. Curtin, L. G. Hector, Jr., and C. F. Woodward, Nat. Mater. **9**, 750 (2010).
[3] D. R. Trinkle and C. Woodward, Science **310**, 1665 (2005).
[4] M. Sluiter, Y. Hashi, and Y. Kawazoe, Comput. Mater. Sci. **14**, 283 (1999).
[5] M. Chandran and S. K. Sondhi, Modell. Simul. Mater. Sci. Eng. **19**, 025008 (2011).
[6] O. I. Gorbatov, I. L. Lomaev, Y. N. Gornostyrev, A. V. Ruban, D. Furrer, V. Venkatesh, D. L. Novikov, and S. F. Burlatsky, Phys. Rev. B **93**, 224106 (2016).
[7] P. E. A. Turchi, G. M. Stocks, W. H. Butler, D. M. Nicholson, and A. Gonis, Phys. Rev. B **37**, 5982 (1988).
[8] J. B. Liu and D. D. Johnson, Mater. Res. Innovations **18**, S4-1021 (2014).
[9] J. E. Saal and C. Wolverton, Acta Mater. **103**, 57 (2016).
[10] M. Asta and A. A. Quong, Philos. Mag. Lett. **76**, 331 (1997).
[11] R. Sun and A. van de Walle, CALPHAD: Comput. Coupling Phase Diagrams Thermochem. **53**, 20 (2016).
[12] P. Hohenberg and W. Kohn, Phys. Rev. **136**, B864 (1964).
[13] W. Kohn and L. J. Sham, Phys. Rev. **140**, A1133 (1965).
[14] J. P. Perdew, K. Burke, and M. Ernzerhof, Phys. Rev. Lett. **77**, 3865 (1996).
[15] J. P. Perdew, K. Burke, and M. Ernzerhof, Phys. Rev. Lett. **78**, 1396 (1997).
[16] G. Kresse and J. Hafner, Phys. Rev. B **47**, 558 (1993).
[17] G. Kresse and J. Hafner, Phys. Rev. B **49**, 14251 (1994).
[18] G. Kresse and J. Furthmüller, Phys. Rev. B **54**, 11169 (1996).
[19] G. Kresse and J. Furthmüller, Comput. Mater. Sci. **6**, 15 (1996).
[20] P. E. Blöchl, Phys. Rev. B **50**, 17953 (1994).
[21] G. Kresse and D. Joubert, Phys. Rev. B **59**, 1758 (1999).
[22] C. Wolverton and A. Zunger, Phys. Rev. B **59**, 12165 (1999).
[23] H. J. Monkhorst and J. D. Pack, Phys. Rev. B **13**, 5188 (1976).
[24] J. M. Sanchez, F. Ducastelle, and D. Gratias, Phys. A (Amsterdam, Neth.) **128**, 334 (1984).
[25] A. van de Walle, M. Asta, and G. Ceder, CALPHAD: Comput. Coupling Phase Diagrams Thermochem. **26**, 539 (2002).
[26] A. van de Walle, CALPHAD: Comput. Coupling Phase Diagrams Thermochem. **33**, 266 (2009).

[27] A. van de Walle, G. Ceder, and U. V. Waghmare, Phys. Rev. Lett. **80**, 4911 (1998).

[28] T. Kruml, J. L. Martin, and J. Bonneville, Philos. Mag. A **80**, 1545 (2000).

[29] G. Pilania, C. Wang, X. Jiang, S. Rajasekaran, and R. Ramprasad, Sci. Rep. **3**, 2810 (2013).

[30] C. Woodward, A. van de Walle, M. Asta, and D. R. Trinkle, Acta Mater. **75**, 60 (2014).

[31] J. B. Liu, D. D. Johnson, and A. V. Smirnov, Acta Mater. **53**, 3601 (2005).

[32] R. Sun and D. D. Johnson, Phys. Rev. B **87**, 104107 (2013).